

Influence of Hydrogen Content on Microstructure and Crystallographic Orientation of Hydrides in Recrystallized Zr-Sn-Nb Tubes

Zeng Wen^{1,2}, Qiu Risheng¹, Luan Baifeng¹, Tao Boran¹, Liu Qing¹, Murty Korukonda L³, Peng Sheng⁴, Wang Ben⁴, Gao Bo⁴, Fang Qiang⁵

¹ Chongqing University, Chongqing 400044, China; ² Chongqing University of Science and Technology, Chongqing 401331, China; ³ North Carolina State University, Raleigh, NC 27695-7909, USA; ⁴ State Nuclear BAOTI Zirconium Industry Company, Baoji 721013, China; ⁵ Panzhihua Iron and Steel Research Institute, Panzhihua 617000, China

Abstract: Although there are many studies on the hydrides in zirconium alloys, the microstructure and crystallographic orientation of hydrides with higher hydrogen content have received little attention. The Zr-Sn-Nb alloy was charged with 147, 340 and 1480 $\mu\text{g/g}$ hydrogen by a gaseous hydriding procedure at 400 °C for different holding time. The microstructure and crystallographic orientation of hydrides were investigated by a combination of optical microscopy (OM), scanning electron microscope (SEM), transmission electron microscopy (TEM) and electron backscatter diffraction (EBSD) techniques. The results indicate that the orientation is affected by the hydrogen content. The interphase boundary components are used to evaluate the crystallographic orientation of hydrides and pole figure analyses. There are two orientation relationships between the α -Zr and the hydrides, namely $(0001)_\alpha // \{111\}_\delta$ and $\{10\bar{1}7\}_\alpha // \{111\}_\delta$. EBSD analyses also reveal the changes in orientation of hydrides when hydrides grow from one matrix grain to another to accommodate the matrix modification. Besides, many Zr grains have both inter-granular and intra-granular hydrides, and only the intra-granular hydrides exhibit a habit relationship with the Zr grains.

Key words: Zr alloy; hydride; crystallographic orientation; habit plane; hydrogen content

Zirconium alloys are widely used in nuclear water reactors as cladding materials because of their low thermal neutron absorption cross-section, good mechanical properties and corrosion resistance at high temperatures. The cladding materials will absorb hydrogen from high temperature water during the operation of nuclear reactor. However, the solubility of hydrogen in zirconium alloys is very limited, and hydrides precipitate when the hydrogen concentration exceeds the terminal solid solubility^[1-4]. Zirconium hydrides are extremely brittle at all temperatures, which reduces the ductility of zirconium alloy and ultimately leads to embrittlement and fracture of the cladding materials^[5].

There are four types of hydrides formed, identified as:

ZrH_{0.5}- ζ , ZrH- γ , ZrH_{1.5-1.7}- δ and ZrH₂- ϵ ^[6]. The majority of experimental studies are about δ -hydrides and γ -hydrides, since they are the hydride phases which are most liable to embrittlement and fracture for cladding materials. Besides, δ -hydrides are the most common hydride phase formed in zirconium alloys at relatively low cooling rates^[7-9]. It is known that hydride orientation will influence the mechanical properties of materials; for example, radial orientated hydrides can drastically reduce the ductility of Zr alloy tubes in contrast to circumferentially oriented ones^[10-13]. Therefore, the orientations of δ -hydrides and γ -hydrides in Zr alloys are extensively studied. It is reported that there are many habit planes for δ -hydrides and γ -hydrides in Zr

Received date: May 25, 2018

Foundation item: National Natural Science Foundation of China (51371202, 51421001, 51531005, 51401187)

Corresponding author: Qiu Risheng, Ph. D., Associate Professor, School of Materials Science and Engineering, Chongqing University, Chongqing 400030, P. R. China, Tel: 0086-23-65106067, E-mail: rsqiu@cqu.edu.cn

Copyright © 2019, Northwest Institute for Nonferrous Metal Research. Published by Science Press. All rights reserved.

alloys^[14, 15]. The reported habit planes for γ -hydrides are mostly $\{10\bar{1}7\}$ and a few (0001)^[16]. For δ -hydrides, the reported habit planes are mainly (0001)^[16-27] and a few $\{10\bar{1}7\}$, while the latter found as inter-granular hydrides^[23, 24]. Many studies have shown that the hydrogen content has a significant influence on hydride precipitation, reorientation and mechanical properties^[28-31]. So far, however, the hydrogen contents of most hydride habit plane studies are between 100~300 $\mu\text{g/g}$, and each hydride is treated as a single entity with a unique habit plane. Such treatment does not consider the orientation variations within a hydride, and the total number of hydrides studied is restricted by the low hydrogen content. Therefore, further investigations are still required to investigate the microstructure and crystallographic orientation of hydrides in Zr alloys with higher hydrogen content ($>300 \mu\text{g/g}$). In this work, interphase boundary components reconstructed by Channel 5 software are used to study the crystallographic orientation of hydrides and pole figure analysis. The interphase boundary components show that the boundaries between α -Zr matrix and hydrides deviate from known orientation relationships in the EBSD map.

1 Experiment

The as-received Zr-Sn-Nb tube was used in this study and the chemical composition is given in Table 1. The tube was charged with hydrogen by a gaseous hydriding procedure using a high pressure hydrogen gas furnace. First, the tube was pickled in a solution with composition of 3% HF, 39% HNO₃ and 58% H₂O. The chamber with the experimental tubes was then filled with hydrogen gas and heated to 400 °C. In order to obtain three different hydrogen contents, the tubes were soaked at 400 °C for three holding time periods followed by furnace cooling (about 0.5 °C/min) to acquire stable hydrides. The H concentrations of the specimens were measured to be about 147, 340 and 1480 $\mu\text{g/g}$ in a hydrogen analyzer (LECO RH-600) using an inert gas fusion method.

Three directions were selected for representing the tube reference frames as shown in Fig.1, where AD denotes axial direction, TD denotes tangential direction and RD denotes radial direction. Table 2 shows the texture parameter f values of the tube evaluated by EBSD.

The tubes were characterized by optical microscopy (OM, Zeiss Axio Imager, Germany), electron backscatter diffraction (EBSD, TESCAN MIRA 3 XMU, Czech) and transmission electron microscopy (TEM, TECNAI G² F20, USA). For OM observation, the samples were polished and

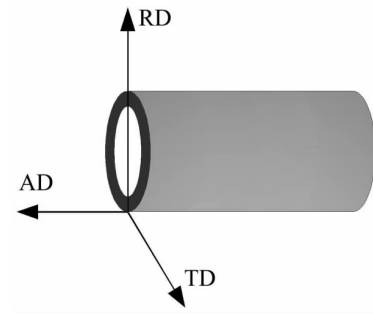


Fig.1 Schematic representation of the tube reference frame

Table 2 Microtexture parameters of Zr-Sn-Nb tube measured by EBSD technique

| f_{AD} | f_{TD} | f_{RD} |
|----------|----------|----------|
| 0.046 | 0.331 | 0.623 |

etched in a solution of 10% HF, 10% H₂O₂ and 80% HNO₃. Samples for EBSD were prepared by the standard metallographic polishing followed by electrolytic polishing in a solution containing 70% CH₃OH, 20% CH₃(CH₂)₃O (CH₂)₂OH and 10% HClO₄ at -30 °C. The TEM samples were obtained by jet polishing in a solution of 10% HClO₄ and 90% CH₃CH₂OH. Bright field image and selected area electron diffraction (SAED) analyses of the Zr matrix grains and hydrides were obtained from samples with 340 and 1480 $\mu\text{g/g}$ H, and the high resolution lattice images were obtained from samples with 340 $\mu\text{g/g}$ H.

2 Results and Discussion

2.1 Optical analysis of hydrides

Fig.2 shows the optical images of samples with different hydrogen contents. It is clear that most hydrides are oriented in tangential direction and the number of radial hydrides increases with increasing the hydrogen content. For sample with 147 $\mu\text{g/g}$ H, the hydrides consist of long tangential hydrides spaced apart and very few radial hydrides near the outside region. When the hydrogen content reaches 340 $\mu\text{g/g}$, the number of hydrides increases with the slightly messy hydride distribution due to the increase in the number of radial hydrides. As the hydrogen content reaches 1480 $\mu\text{g/g}$, a large number of radial hydrides precipitate and form a fully inter-linked hydride configuration. It is worthwhile noting that some hydrides consist of several very closely positioned parallel hydride platelets, indicating that these hydrides share a common habit plane^[20, 26, 32-33].

2.2 TEM analysis of hydrides

Fig.3 includes the TEM images and SAED patterns of hydrides in tubes with 340 and 1480 $\mu\text{g/g}$ H. It is noted that there are stress fringes near hydrides, as shown in Fig.3a, due to the volume expansion, and the precipitation of γ and δ phases

Table 1 Chemical composition of Zr-Sn-Nb tube (wt%)

| Sn | Nb | Fe | Cr | Cu | Zr |
|------|-----|------|------|------|------|
| 0.85 | 0.3 | 0.35 | 0.15 | 0.05 | Bal. |

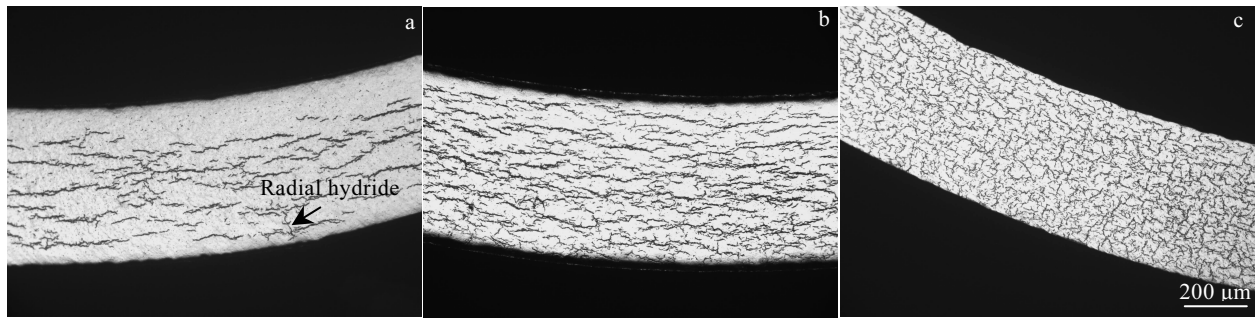


Fig.2 OM images of hydrogenated tubes with 147 $\mu\text{g/g}$ H (a), 340 $\mu\text{g/g}$ H (b), and 1480 $\mu\text{g/g}$ H (c)

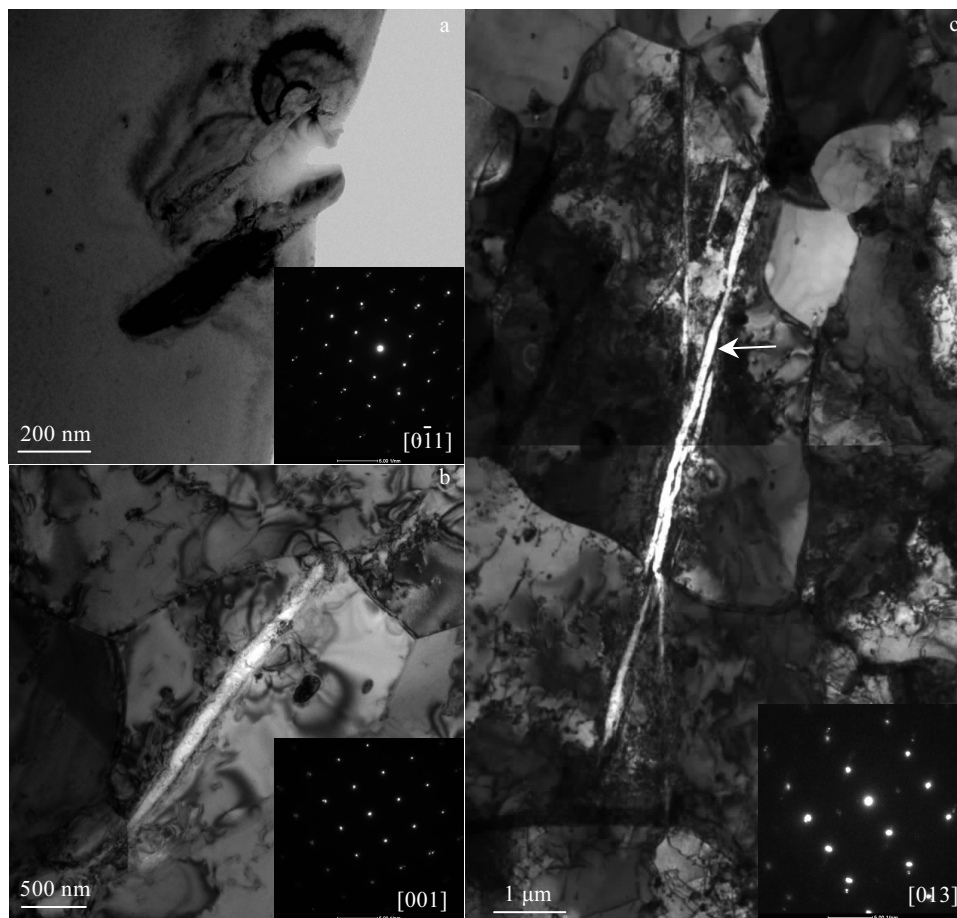


Fig.3 TEM images and corresponding SAED patterns of hydrides in tube with 340 $\mu\text{g/g}$ H (a) and 1480 $\mu\text{g/g}$ H (b, c)

in $\alpha\text{-Zr}$ is reported to be 12.3% and 17.6%, respectively^[34-38]. With respect to the hydride precipitation locations, hydrides can be classified into three types, namely intra-granular, inter-granular and trans-granular hydrides^[39]. It is clear from Fig.3a that the hydrides within grains (intra-granular hydrides) have a strip shape and a size of about 400~800 nm. However, the size of intragranular hydrides in tube with 1480 $\mu\text{g/g}$ H is about 2.5 μm (Fig.3b), which is much larger than that in tube with 340 $\mu\text{g/g}$ H. The trans-granular hydrides are found in tube with 1480 $\mu\text{g/g}$ H, as shown in Fig.3c. It is

clear that the trans-granular hydrides are very long, extending about 5~10 μm , and there are several hydrides growing together along the same growth direction.

Fig.4 shows the high resolution lattice image of $\alpha\text{-Zr}$ and intra-granular hydride in Fig.3a, and the hydride phase is noted to be $\delta\text{-ZrH}_{1.66}$ with $d_{(111)}=0.276$ nm and $d_{(200)}=0.241$ nm, as verified from the inverse fast Fourier transform (FFT).

Fig.5 illustrates the TEM image and SAED patterns in tube with 1480 $\mu\text{g/g}$ H. There are two kinds of diffraction patterns, namely, electron diffraction pattern of the fcc δ -hydride (red

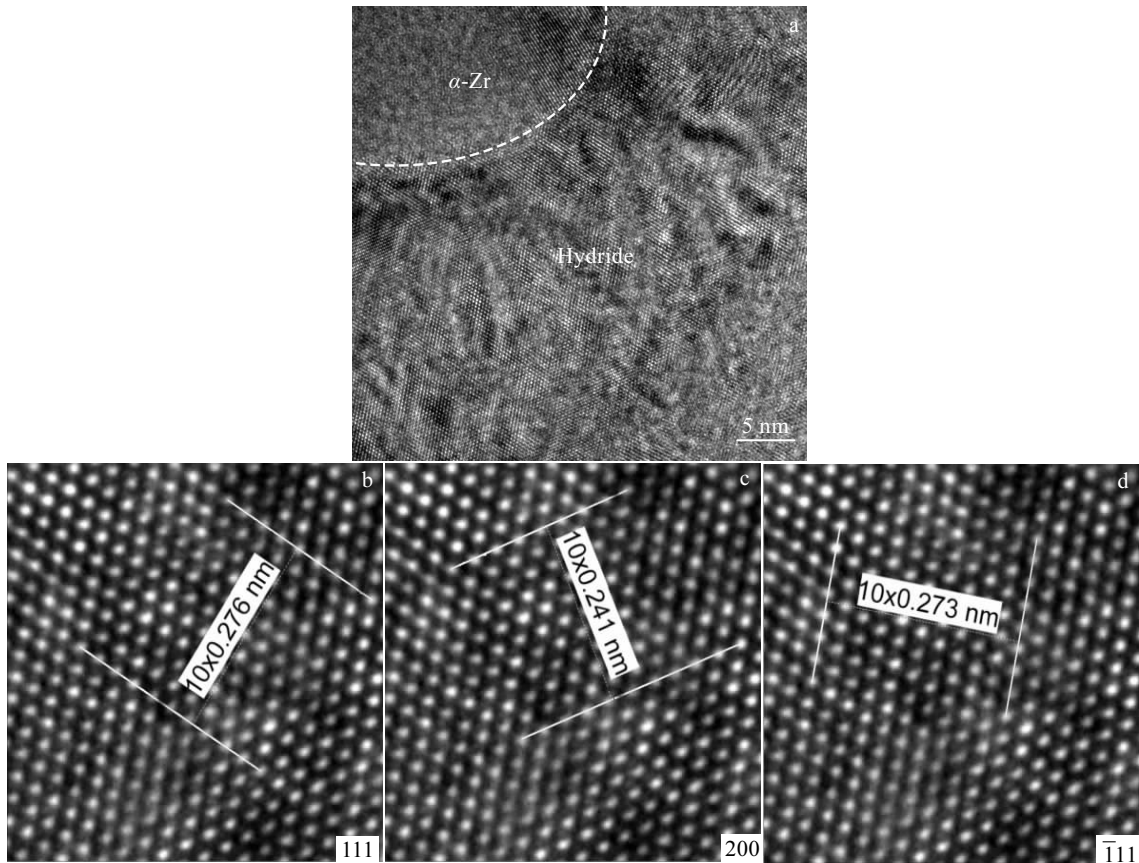


Fig.4 HRTEM lattice image (a) and inter-planar distances based on inverse FFT (b-d) of the hydride in Fig.3a

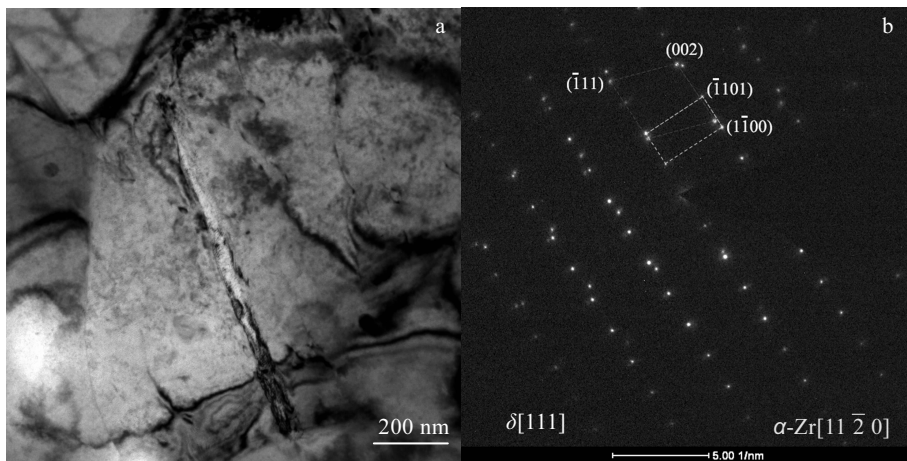


Fig.5 TEM image (a) and corresponding SAED patterns (b) of the hydride (red lines) and α -Zr matrix (yellow lines) in tube with 1480 $\mu\text{g/g}$ H

lines) and hexagonal α -Zr matrix (yellow lines), as shown in Fig.5b. Based on the diffraction patterns, it is concluded that the relation between the α -Zr matrix and the fcc δ -hydride is $(0001)_\alpha // \{111\}_\delta$ and $[11\bar{2}0]_\alpha // [110]_\delta$.

2.3 EBSD analysis of hydrides

The results from TEM analysis as well as the Kikuchi pattern indexed by the EBSD system using ICSD [56198] indicate that the hydrides in the tube are δ -ZrH_{1.66} (δ -ZrH_x, space

group: Fm $\bar{3}$ m). The EBSD analysis is divided into the following five categories.

(1) Hydride morphology and position

Fig.6a, 6c and 6d depict the EBSD maps of tube samples with 147, 340 and 1480 $\mu\text{g/g}$ H hydrogen, respectively. The figures are plotted in such a way that the crystallographic orientations of different zirconium grains are marked with different colors according to the Euler angle color map, and

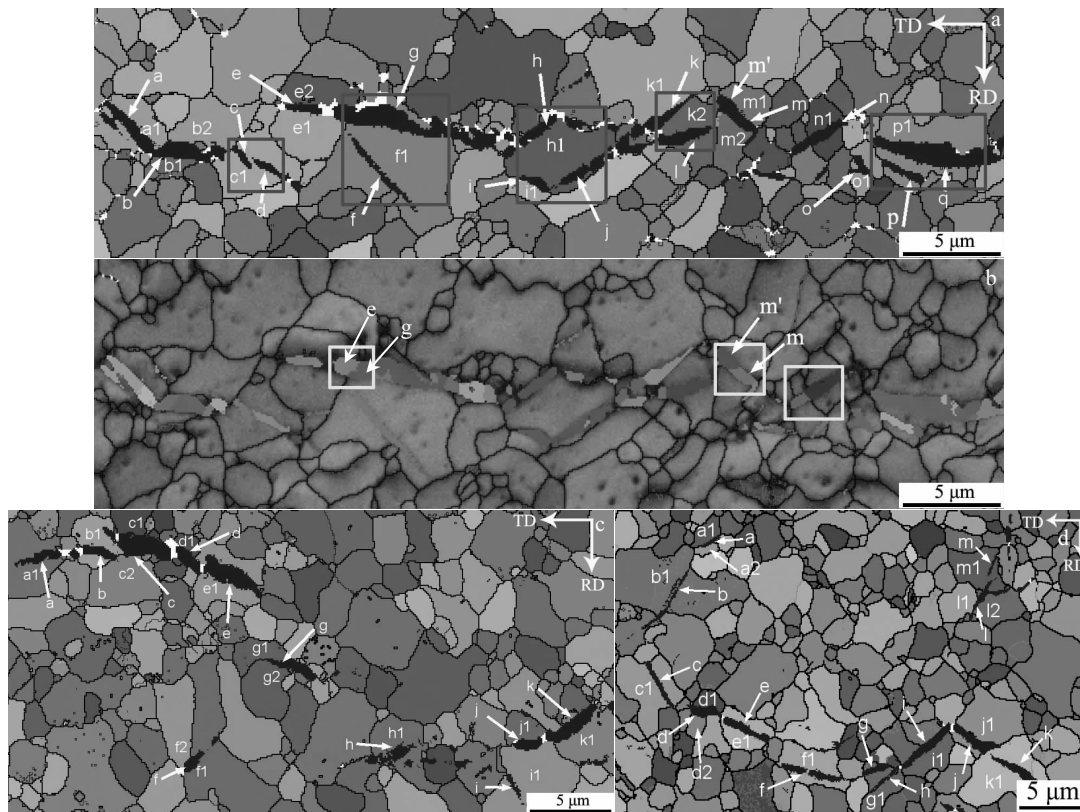


Fig.6 EBSD maps of α -Zr and hydrides in tube with 147 $\mu\text{g/g}$ H (a, b), 340 $\mu\text{g/g}$ H (c), and 1480 $\mu\text{g/g}$ H (d) (in Fig.8a, 8c and 8d, α -Zr is all Euler and δ -ZrH_x is navy blue (white areas represent areas not indexed by EBSD); in Fig.8b α -Zr is band contrast and δ -ZrH_x is all Euler)

hydrides are marked with navy blue. As shown in Fig.6a, the hydrides are oriented in tangential direction (TD) and linked with each other to form a hydride string in the sample with 147 $\mu\text{g/g}$ H. The hydride string disappears in the sample with 340 $\mu\text{g/g}$ H (Fig.6c) while the tangential distribution is still visible. The tangential distribution is replaced by an interlinked hydride network in the sample with 1480 $\mu\text{g/g}$ H (Fig.6d), which has an additional population of radial hydrides.

(2) Habit plane of intra-granular hydrides

The crystallographic relationships between a micron-sized hydride and its surrounding Zr grains were analyzed by comparing the stereographic projections of the corresponding crystal plane poles, as shown in Table 3. The poles of a few selected grains are shown in Fig.7. All of the matrix grains with the surrounding intra-granular hydrides have an orientation relationship of $(0001)_\alpha // \{111\}_\delta$.

(3) Habit plane of inter-granular hydrides

The crystallographic relationships between inter-granular hydrides and the surrounding zirconium grains were also analyzed, and the results show that inter-granular hydrides do not have the two orientation relationships with all of its neighboring zirconium grains (Table 3). Interestingly, there

are many zirconium grains that have both inter-granular and intra-granular hydrides. As shown in Fig.7, the zirconium grains only have an orientation relationship with the intra-granular hydrides and do not have any orientation relationship with the inter-granular hydrides.

(4) Habit plane of trans-granular hydrides

Fig.6b is Euler map of hydrides, which reveals that all the trans-granular hydrides (g and e, m and m' in Fig.6b) have an $(0001)_\alpha // \{111\}_\delta$ orientation relationship with the matrix grains. Since grains have different orientations, the trans-granular hydrides must be reoriented when they grow from one grain into another to accommodate the matrix/orientation change. This implies that trans-granular hydrides are several physically connected hydrides within different zirconium grains.

(5) Distribution of the angle between hydride $\{111\}$ plane and each of the two zirconium planes

In this work, we used interphase boundary components in Channel 5 software to study the crystallographic orientation of hydrides. The angles between hydride $\{111\}_\delta$ and zirconium $(0001)_\alpha$ planes along the phase boundaries are shown in Fig.8a, where the α -Zr phase is marked with red color and the

δ -hydride phase is marked with blue. The phase boundaries with a deviation up to 5.5° from the specified orientation relationships are shown in white, while those above 5.5° is shown in yellow. Similar plot for hydride $\{111\}_\delta$ and zirconium $\{10\bar{1}7\}_a$ planes is shown in Fig.8b. Angular distributions are illustrated in Fig.8c and Fig.8d. The average deviation angle between hydride $\{111\}_\delta$ and zirconium $\{10\bar{1}7\}_a$ planes is much larger than that between hydride $\{111\}_\delta$ and zirconium $(0001)_a$ plane, which indicates that most hydrides have the orientation relationship of $(0001)_a // \{111\}_\delta$. The proportion of the phase boundaries smaller than 5.5° deviation is 76.38% for the orientation relationship of $(0001)_a // \{111\}_\delta$ and is 4.57% for the orientation relationship of

$\{10\bar{1}7\}_a // \{111\}_\delta$, as given in Table 4. The sum of the two is less than 100%, so there should be other relationships apart from the above mentioned orientation relationships, which agrees with other reports^[14, 15]. The analysis was also conducted on the tube samples with 340 and 1480 $\mu\text{g/g}$ H, and similar conclusion was obtained, and the results are summarized in Table 4. All of the hydrides except the one that we analyzed by pole figure method maintain the relationship of $(0001)_a // \{111\}_\delta$, as shown in Table 4. However, the phase boundary deviation distributions of the orientation relationships of $(0001)_a // \{111\}_\delta$ and $\{10\bar{1}7\}_a // \{111\}_\delta$ indicate that there may be other orientation relationships, albeit rarely^[15, 40].

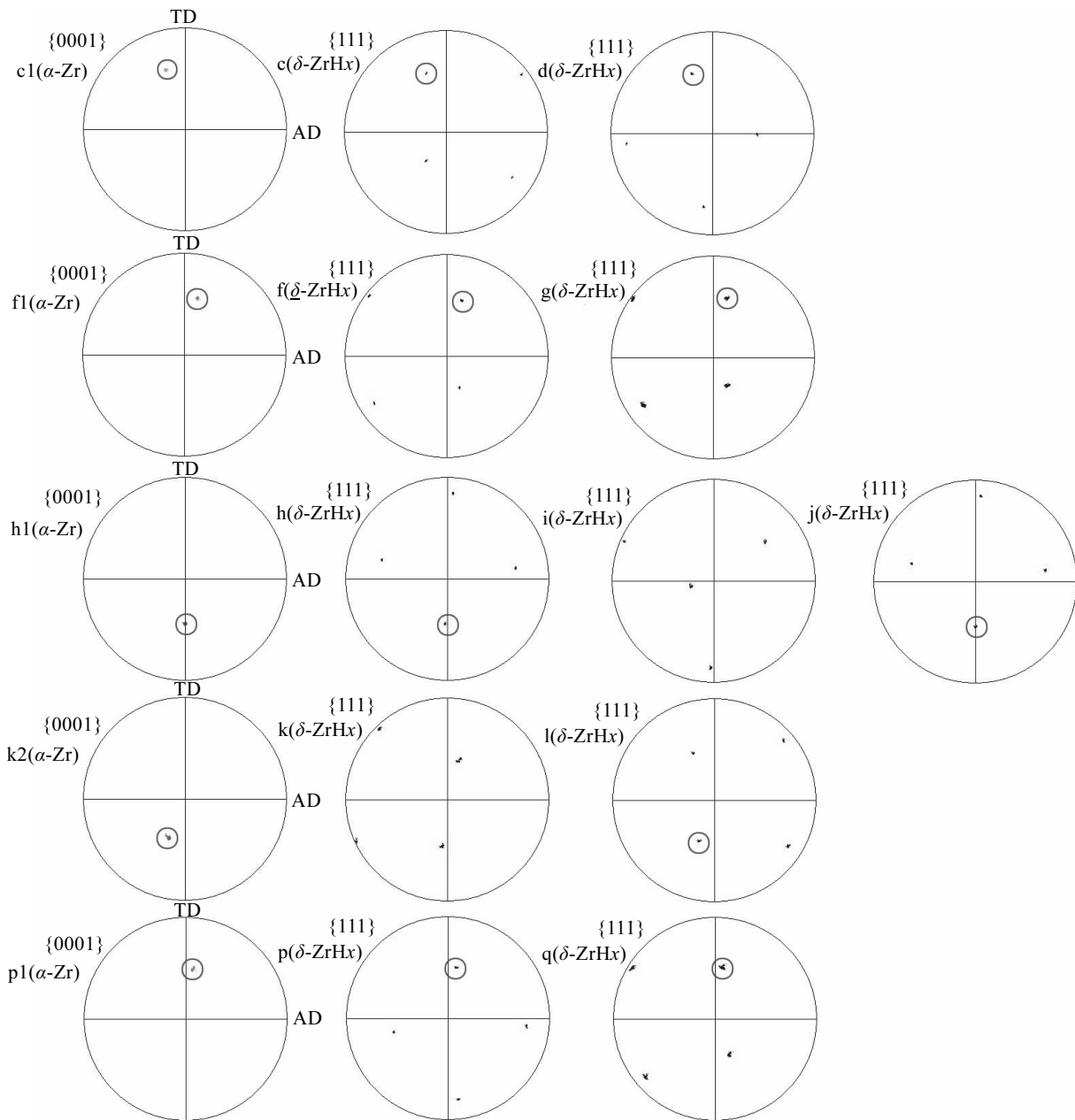


Fig.7 Pole figures of the Zr matrix and hydrides (red box) in Fig.6a

Table 3 Results of crystallographic relationships between α -Zr and δ -ZrH_x obtained by EBSD

| Hydrogen content/ $\mu\text{g}\cdot\text{g}^{-1}$ | Figure | Location (α -Zr) | Location (δ -ZrH _x) | Precipitation site | Crystallographic relationship |
|---|--------|--------------------------|---|--------------------|--|
| 147 | Fig.6a | a1 | a | Intra-granular | (0001) _{a1} //(111) _a |
| | | b1, b2 | b | Inter-granular | (0001) _{b1} //(111) _b |
| | | c1 | c | Intra-granular | (0001) _{c1} //(111) _c |
| | | e1 | d | Intra-granular | (0001) _{e1} //(111) _d |
| | | e1, e2 | e | Inter-granular | (0001) _{e2} //(111) _e |
| | | f1 | f | Intra-granular | (0001) _{f1} //(111) _f |
| | | f1 | g | Intra-granular | (0001) _{f1} //(111) _g |
| | | h1 | h | Intra-granular | (0001) _{h1} //(111) _h |
| | | i1 | i | Inter-granular | (0001) _{i1} //(111) _i |
| | | h1 | j | Intra-granular | (0001) _{h1} //(111) _j |
| | | k1, k2 | k | Inter-granular | (0001) _{k1} //(111) _k |
| | | k2 | l | Intra-granular | (0001) _{k2} //(111) _l |
| | | m1 | m' | Inter-granular | (0001) _{m1} //(111) _{m'} |
| | | m2 | m | Inter-granular | (0001) _{m2} //(111) _m |
| | | n1 | n | Intra-granular | (0001) _{n1} //(111) _n |
| | | o1 | o | Intra-granular | (0001) _{o1} //(111) _o |
| p1 | p | Intra-granular | (0001) _{p1} //(111) _p | | |
| p1 | q | Intra-granular | (0001) _{p1} //(111) _q | | |
| 340 | Fig.6c | a1 | a | Intra-granular | (0001) _{a1} //(111) _a |
| | | b1 | b | Intra-granular | (0001) _{b1} //(111) _b |
| | | c1, c2 | c | Inter-granular | (0001) _{c1} //(111) _c |
| | | d1 | d | Intra-granular | (0001) _{d1} //(111) _d |
| | | e1 | e | Intra-granular | (0001) _{e1} //(111) _e |
| | | f1, f2 | f | Inter-granular | (0001) _{f1} //(111) _f |
| | | g1, g2 | g | Inter-granular | (0001) _{g1} //(111) _g |
| | | h1 | h | Intra-granular | (0001) _{h1} //(111) _h |
| | | i1 | i | Intra-granular | (0001) _{i1} //(111) _i |
| | | j1 | j | Inter-granular | (0001) _{j1} //(111) _j |
| | | k1 | k | Intra-granular | (0001) _{k1} //(111) _k |
| 1480 | Fig.6d | a1, a2 | a | Inter-granular | (0001) _{a1} //(111) _a |
| | | b1 | b | Intra-granular | (0001) _{b1} //(111) _b |
| | | c1 | c | Intra-granular | (0001) _{c1} //(111) _c |
| | | d1, d2 | d | Inter-granular | (0001) _{d1} //(111) _d |
| | | e1 | e | Intra-granular | (0001) _{e1} //(111) _e |
| | | f1 | f | Intra-granular | (0001) _{f1} //(111) _f |
| | | g1 | g | Intra-granular | (0001) _{g1} //(111) _g |
| | | g1 | h | Intra-granular | (0001) _{g1} //(111) _h |
| | | i1 | i | Intra-granular | (0001) _{i1} //(111) _i |
| | | j1 | j | Intra-granular | (0001) _{j1} //(111) _j |
| | | k1 | k | Intra-granular | (0001) _{k1} //(111) _k |
| l1, l2 | l | Inter-granular | (0001) _{l2} //(111) _l | | |
| m1 | m | Intra-granular | (0001) _{m1} //(111) _m | | |

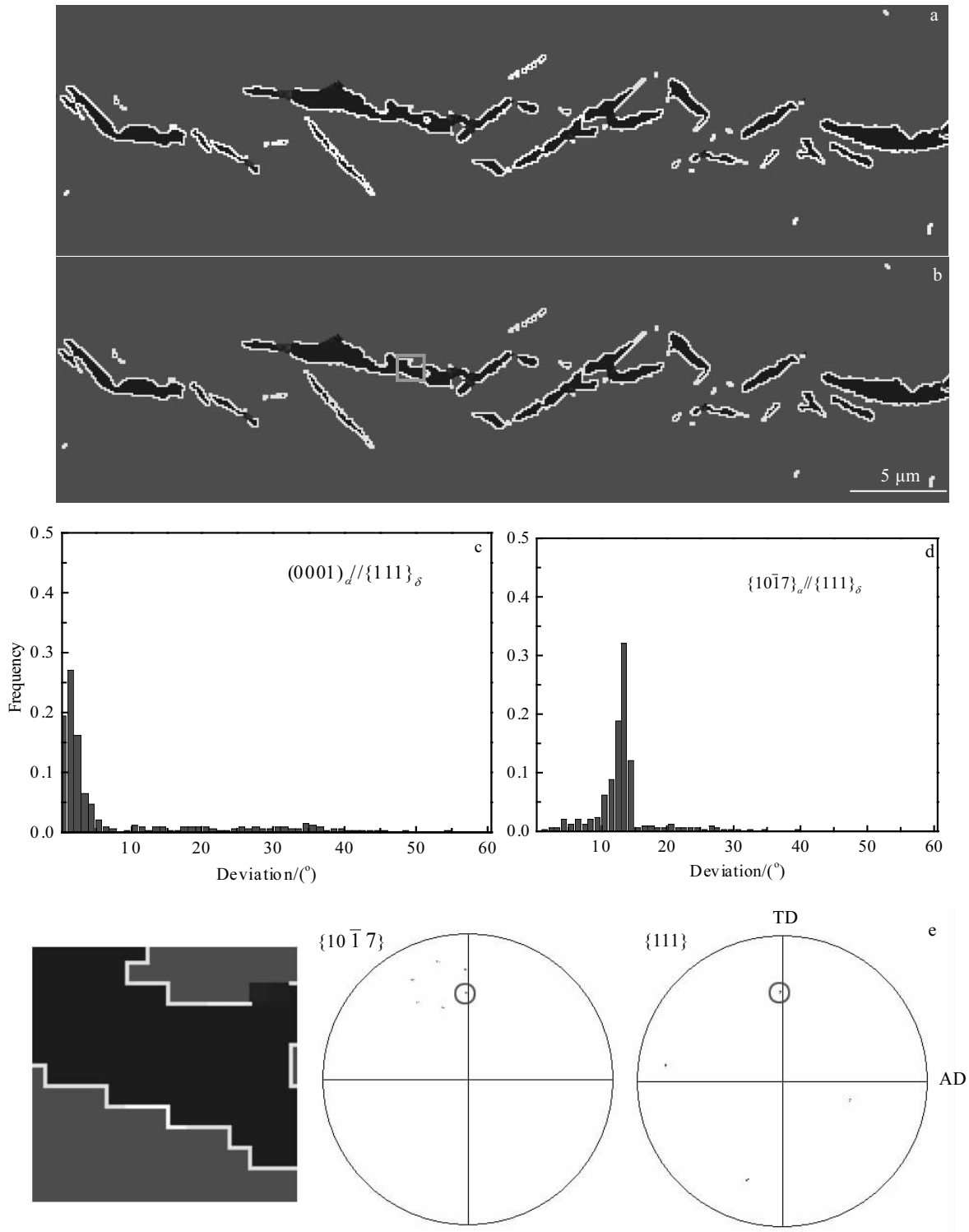


Fig.8 Phase maps of phase boundaries with the orientation relationships of (0001)_a//{111}_δ (a) and {10 $\bar{1}$ 7}_a//{111}_δ (b) of tube with 147 μg/g H (the boundaries with a deviation below 5.5° from the specified orientation relationships are shown by white and those above 5.5° are shown by yellow; the α-Zr phase is shown by red and the hydride phase is shown by blue); phase boundary deviation distribution of Fig.8a (c) and Fig.8b (d); pole figures of a hydride and the surrounding α-Zr matrix marked with green box in Fig.8b (e) (the black areas in Fig.8a, 8b and 8e represent areas not indexed by EBSD)

Table 4 Proportion of the phase boundaries deviated below 5.5° from the known orientation relationships

| Hydrogen content/ $\mu\text{g}\cdot\text{g}^{-1}$ | $(0001)_\alpha // \{111\}_\delta / \%$ | $\{10\bar{1}7\}_\alpha // \{111\}_\delta / \%$ |
|---|--|--|
| 147 | 76.38 | 4.57 |
| 340 | 77.77 | 1.92 |
| 1480 | 83.75 | 2.62 |

3 Conclusions

1) The hydride phases in recrystallized Zr-Sn-Nb tubes are identified as fcc δ -ZrH_{1.66}. The hydrides in tubes with 147 and 340 $\mu\text{g/g}$ H are mostly tangentially oriented, and large amounts of radial hydrides only appear in tubes with 1480 $\mu\text{g/g}$ H. The α -Zr matrix and the δ -hydride have a primary orientation relationship of $(0001)_\alpha // \{111\}_\delta$ and $[11\bar{2}0]_\alpha // [110]_\delta$.

2) The most common habit relationships between hydrides and Zr matrix are $(0001)_\alpha // \{111\}_\delta$ and $\{10\bar{1}7\}_\alpha // \{111\}_\delta$. However, the hydrides with the former orientation predominate and increase slightly with increasing the hydrogen content.

3) The orientation of hydrides changes when they grow from one matrix grain to another to accommodate the difference in matrix orientation. Furthermore, there are many Zr grains with both inter-granular and intra-granular hydrides. The Zr grains only have orientation relationships with the intra-granular hydrides and have no relationship with the inter-granular hydrides.

References

- Northwood D O, Kosasih U. *International Metals Reviews*[J], 1983, 28(1): 92
- Puls M P. *Acta Metallurgica*[J], 1981, 29(12): 1961
- Puls M P. *Acta Metallurgica*[J], 1984, 32(8): 1259
- Zuzek E, Abriata J P, San-Martin A et al. *Bulletin of Alloy Phase Diagrams*[J], 1990, 11(4): 385
- Simpson L A, Cann C D. *Journal of Nuclear Materials*[J], 1979, 87(2-3): 303
- Bair J, Zaeem M A, Tonks M. *Journal of Nuclear Materials*[J], 2015, 466: 12
- Nath B, Lorimer G W, Ridley N. *Journal of Nuclear Materials*[J], 1975, 58(2): 153
- Bradbrook J S, Lorimer G W, Ridley N. *Journal of Nuclear Materials*[J], 1972, 42(2): 142
- Nath B, Lorimer G W, Ridley N. *Journal of Nuclear Materials*[J], 1974, 49(3): 262
- Chu H C, Wu S K, Chien K F et al. *Journal of Nuclear Materials*[J], 2007, 362(1): 93
- Sharma R K, Sunil S, Kumawat B K et al. *Journal of Nuclear Materials*[J], 2017, 488: 231
- Muta H, Nishikane R, Ando Y et al. *Journal of Nuclear Materials*[J], 2017, 500: 145
- Auzoux Q, Bouffieux P, Machiels A et al. *Journal of Nuclear Materials*[J], 2017, 494: 114
- Qin W, Szpunar J A, Kumar N A P K et al. *Acta Materialia*[J], 2014, 81: 219
- Pshenichnikov A, Stuckert J. *International Conference on Nuclear Engineering*, V001T02A006[C]. North Carolina: American Society of Mechanical Engineers, 2016
- Neogy S, Srivastava D, Tewari R et al. *Journal of Nuclear Materials*[J], 2003, 322(2-3): 195
- Kim S D, Kim Y, Kim J S et al. *Journal of Nuclear Materials*[J], 2015, 465(S1): 731
- Kumar N A P K, Szpunar J A, He Z. *Journal of Nuclear Materials*[J], 2010, 403(1): 101
- Qin W, Kumar N A P K, Szpunar J A et al. *Acta Materialia*[J], 2011, 59(18): 7010
- Kumar N A P K, Szpunar J A. *Materials Science & Engineering A*[J], 2011, 528(21): 6366
- Chen L, Wang X, Gong W et al. *International Journal of Hydrogen Energy*[J], 2014, 39(36): 21 116
- Krishna K V, Shodiev D et al. *Journal of Nuclear Materials*[J], 2011, 414(2): 270
- Une K, Ishimoto S. *Journal of Nuclear Materials*[J], 2006, 357(1-3): 147
- Une K, Nogita K, Ishimoto S et al. *Journal of Nuclear Science & Technology*[J], 2004, 41(7): 731
- Yuan Gaihuan, Cao Guoqin, Yue Qiang et al. *Journal of Alloys & Compounds*[J], 2016, 658: 494
- Celiz Z E, Saumell M L, Versaci R A et al. *Procedia Materials Science*[J], 2015, 8: 442
- Rajasekhara S, Kotula P G, Enos D G et al. *Journal of Nuclear Materials*[J], 2016, 489: 222
- Cha H J, Won J J, Jang K N et al. *Journal of Nuclear Materials*[J], 2015, 464(1): 53
- Min S J, Kim M S, Kim K T. *Journal of Nuclear Materials*[J], 2013, 441(1-3): 306
- Desquines J, Drouan D, Billone M. *Journal of Nuclear Materials*[J], 2014, 453(1-3): 131
- Zhou Jun, Li Zhongkui, Zhang Jianjun et al. *Rare Metal Materials & Engineering*[J], 2012, 41(9): 1531
- Tulk E, Kerr M, Daymond M R. *Journal of Nuclear Materials*[J], 2012, 425(1-3): 93
- Perovic V, Weatherly G C, Simpson C J. *Acta Metallurgica*[J], 1983, 31(9): 1381
- Ells C E. *Journal of Nuclear Materials*[J], 1968, 28(2): 129
- Miyake M, Uno M, Yamanaka S. *Journal of Nuclear Materials*[J], 1999, 270(1-2): 233
- Kim Y S, Wang W E, Olander D R et al. *Journal of Nuclear Materials*[J], 1996, 240(1): 27
- Small W M, Root J H, Khatamian D. *Journal of Nuclear Materials*[J], 1998, 256(2-3): 102
- Dupin N, Ansara I, Servant C et al. *Journal of Nuclear Materials*[J], 1999, 275(3): 287
- Zhao Z, Blat-Yrieix M, Morniroli J P et al. *Journal of Astm International*[J], 2008, 5(3): 101 161
- Long F, Kerr D, Domizzi G et al. *Acta Materialia*[J], 2017, 129: 450

氢含量对再结晶 Zr-Sn-Nb 管材氢化物微观结构及取向的影响

曾文^{1,2}, 邱日盛¹, 栾佰峰¹, 陶勃然¹, 刘庆¹, Murty Korukonda L³, 彭胜⁴, 王奔⁴, 高博⁴, 方强⁵

(1. 重庆大学, 重庆 400044)

(2. 重庆科技学院, 重庆 401331)

(3. 北卡罗莱纳州立大学, 美国 北卡罗莱纳州 罗利 27695-7909)

(4. 国核宝钛铝业股份有限公司, 陕西 宝鸡 721013)

(5. 攀枝花钢铁研究院, 四川 攀枝花 617000)

摘要: 虽然已有较多锆合金氢化物的研究, 但对于较高氢含量中锆合金氢化物的研究较少。首先对 Zr-Sn-Nb 管材在 400 °C 下气相渗氢, 通过保温不同时间获得具有 3 种不同氢含量 (147、340、1480 μg/g) 的渗氢样品。随后采用 OM、SEM、TEM 和 EBSD 表征技术, 研究了 Zr-Sn-Nb 管材中氢化物的微观结构与基体的晶体学取向关系。结果表明: 氢含量影响管材中氢化物的取向, α -Zr 基体与氢化物之间存在 $(0001)_\alpha // \{111\}_\delta$ 和 $\{10\bar{1}7\}_\alpha // \{111\}_\delta$ 2 种取向关系。EBSD 分析表明, 氢化物从一个基体晶粒向另一个基体晶粒生长时取向会随着基体晶粒取向的变化而变化。部分锆基体晶粒内同时有晶内氢化物和晶间氢化物, 而只有晶内氢化物与锆基体有晶体学取向关系。

关键词: 锆合金; 氢化物; 晶体学取向; 惯习面; 氢含量

作者简介: 曾文, 男, 1990 年生, 硕士, 讲师, 重庆科技学院冶金与材料工程学院, 重庆 401331, E-mail: wzeng@cqu.edu.cn